Received 8 May 2020; revised 5 June 2020; accepted 6 June 2020. Date of publication 11 June 2020; date of current version 8 July 2020.

Digital Object Identifier 10.1109/OJAP.2020.3001579

A Method for Optimising Superdirectivity of Coupled Meta-Atoms via Planar Directivity Evaluation

JIARUO YAN [1], ANNA RADKOVSKAYA [2,4], SVETLANA KIRIUSHECHKINA [2,3], IRINA KHROMOVA [1,4], CHRISTOPHER STEVENS [1] (Member, IEEE), LASZLO SOLYMAR [1], AND EKATERINA SHAMONINA [1]

[1]Department of Engineering Science, University of Oxford, Oxford OX1 3PJ, U.K.

[2]Magnetism Division, Faculty of Physics, M. V. Lomonosov Moscow State University, 119992 Leninskie Gory, Russia

[3]Grove School of Engineering, City College of New York, New York, NY 10031, USA

[4]Metaboards Limited, Oxford OX2 6HT, U.K.

CORRESPONDING AUTHOR: J. YAN (e-mail: jiaruo.yan@eng.ox.ac.uk)

The work of Jiaruo Yan was supported by Metaboards Ltd., within Russel Studentship Project 'Directivity of Metamaterial-Based Antennas.' The work of Christopher Stevens and Ekaterina Shamonina was supported by the Engineering and Physical Sciences Research Council, U.K., SYMETA under Grant EP/N010493/1.

ABSTRACT We propose a simple and rapid way of optimising directivity in metamaterial-inspired endfire antenna arrays with strong inter-element coupling. We introduce, in addition to the traditional 3D directivity, also its planar equivalents defined as the ratio of the power density in the desired endfire direction to the average power density calculated either in the horizontal (azimuthal) or vertical (elevation) plane. Using dimers of magnetically coupled split-ring resonators with only one element driven by an external source, we derive conditions that must be satisfied in order to realise superdirective current distributions. The superdirective conditions link the quality factor of the resonators and their coupling constant to the array size and the operating frequency. We demonstrate that a rapid measurement in the azimuthal plane can be used as a reliable indicator for whether the superdirective conditions for the 3D directivity are satisfied. Analytical calculations are verified by CST simulations in the MHz frequency range for meta-atoms of circular and square shape. Our method can be extended to arrays comprising larger number of meta-atoms of various shape and would enable rapid prototyping of 3D-printed meta-atoms with desired radiation properties.

INDEX TERMS Superdirective antennas, electromagnetic coupling, electromagnetic metamaterials, electromagnetic radiation.

I. INTRODUCTION

THE CONCEPT of superdirectivity implies that an arbitrarily sharp radiation beam can be produced by a finite size system. The idea was first proposed nearly a century ago by Oseen [1] who referred to 'Einsteinean needle radiation' showing that Maxwell's equations do not contradict the concept, but that in order to achieve superdirectivity a fast spatially varying current distribution within the array is required. Idea of superdirectivity in arrays with a finite number of elements was developed in the 1940's and 1950's. Schelkunoff [2] demonstrated the possibility to design linear antenna arrays that produce arbitrarily sharp beams. Uzkov [3] proved that, for an array of N isotropic radiators, the endfire directivity tends to N^2 as the inter-element distance tends to zero. A treatise for general linear arrays was developed by Bloch *et al.* [4] who derived a closed-form expression of the maximum achievable directivity. Uzsoky and Solymar [5] introduced the concept of tolerance sensitivity, T, and quality factor, Q, to point out the limitations on superdirectivity, and found a closed-form solution for maximum directivity taking into account T and Q. Toraldo di Francia [6] related superdirectivity to optical resolution. Chu [7], Harrington [8] and Pozar [9] explored superdirectivity based on spherical harmonics. Further theoretical studies on optimising the directivity of an antenna array can be found in [10], [11],

[12], [13], [14], [15]. Experimentally, four-element arrays with only one element fed were studied by Bacon and Medhurst [16] and by Newman and Schrote [17]. More recently, experiments on superdirective structures comprising two [18], [19] or three [20] electrically small elements were reported. Directivity of antennas can be increased by using metamaterial-inspired structures [21], [22], [23]. References [24], [25], [26], [27] studied metamaterial superdirective arrays both analytically and experimentally. Ludwig *et al.* [28] considered superdirectivity in studying near-field subwavelength focusing.

What is the physical principle behind superdirectivity? It is best understood when comparing it to a traditional phased array [29]. In a phased array comprising N isotropic elements currents in the array need to be excited in such a way that their fields in the desired direction add up in phase resulting in constructive interference. In the endfire direction of a linear array with elements spaced equidistantly at a distance d the recipe for exciting the phased array would be that the neighbouring currents are excited with a phase shift amounting to kd where $k = 2\pi/\lambda$ is the wave number and λ is the wavelength of the free-space radiation. In contrast, superdirectivity results from destructive interference in all directions but least so in the direction of the main lobe. As the distance between elements tends to zero, the excitation required for superdirectivity means that currents from neighbouring elements of the array are practically in anti-phase [10], [30], [31].

How to impose the required rapidly varying spatial current distribution? One possibility would be to drive separately each element of the array. A variety of approaches were proposed, e.g., by using a tuneable feeding network [18], by incorporating metamaterial-based insulators [21] and metamaterial phase shifting lines [23]. An alternative is born out of the concept of metamaterials with strong inter-element coupling. In dimers comprising resonant meta-atoms only one element is driven and the others are passive [19]. Recent studies [24], [25], [26], [27] provided an explanation that the desired rapid spatial variation of currents required for superdirectivity is imposed via to magnetoinductive waves [32] propagating by virtue of magnetic coupling along chains of coupled meta-atoms. Radkovskaya *et al.* [27] postulated two 'superdirective conditions' that have to be satisfied for two coupled resonators to become superdirective. Superdirective condition 1 (SD_1) states that superdirectivity can only occur very close to the antisymmetric resonance of the dimer, with currents being nearly in anti-phase. Superdirective condition 2 (SD_2) prescribes the relationship between the coupling constant, the quality factor, the operating frequency and the distance between meta-atoms [27].

Whether or not the performance of an array is superdirective requires experimental validation. Often an anechoic chamber is too small to enable far-field measurements, then near-field data are obtained and transformed into far-field data. The common techniques include planar, cylindrical, and spherical near-field measurements [33], [34], [35]. The directivity being defined as the ratio of the power density in the desired direction and the density averaged over the solid angle of 4π implies that the power density is being experimentally captured in all spatial directions. Apart from the fact that such a measurement requires a sophisticated apparatus, to collect data in all spatial directions is a lengthy procedure.

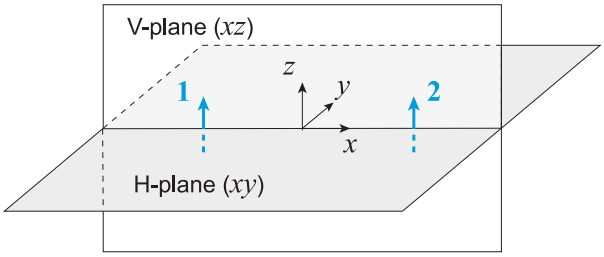

FIGURE 1. Schematic representation of a dimer of meta-atoms modelled as magnetic dipoles. Planar directivities D_H and D_V are determined in the azimuthal H-plane and in the elevation V-plane.

In this paper we propose an alternative approach - to rely on planar measurements of the directivity defined in two planes, the horizontal (azimuthal) and the vertical (elevation) planes. We formulate the design rules for optimising superdirective endfire arrays of coupled meta-atoms by deriving superdirective conditions SD_1 and SD_2 for planar measurements. We prove that planar measurements can be used as a reliable guide for optimisation of the overall 3D directivity, both in terms of the optimum operating frequency and of the optimum distance between the resonators, and verify our approach with CST simulations for resonators of various shape.

The structure of the paper is as follows. In Section II we develop the concept of planar directivity and compare the required current distributions that result in 3D superdirectivity and planar superdirectivity. In Section III we find the conditions required to realise the desired optimum current distribution in a dimer of resonant meta-atoms treated as a pair of interacting magnetic dipoles. We derive the analytical 'superdirective conditions' for 3D and for planar directivity and prove that the latter is a suitable indicator for achieving the former. The model is verified in Section IV by numerical simulations for resonators of circular and square shape resonant in the MHz frequency range. Conclusions are drawn in Section V. Details of mathematical derivations are presented in the Appendices, in order not to interrupt the flow of argument.

II. OPTIMISED 3D DIRECTIVITY AND PLANAR DIRECTIVITIES

A schematic diagram of two coupled meta-atoms is shown in Fig. 1, with elements arranged along the x axis at a distance d being approximated as two vertical magnetic dipole radiators oriented along the z axis. The elements we have in mind are resonant capacitively loaded split-ring resonators that are coupled magnetically, as will be discussed later in Section III. The horizontal azimuthal plane (xy plane) shall be denoted as H-plane and the vertical elevation plane (xz plane) shall be denoted as V-plane.

In analogy to the classical 3D directivity defined as the ratio of the power density in the desired direction to its value averaged over the solid angle 4π,

$$D_{3D} = \frac{P_{max}}{\langle P \rangle_{\text{solid angle}}} \tag{1}$$

we define planar directivities D_H and D_V as the ratio of the power density in the desired direction over the average power density in the selected (V- and H-) planes, i.e.,

$$D_H = \frac{P_{max}}{\langle P \rangle_{\text{H-plane}}} \text{ and } D_V = \frac{P_{max}}{\langle P \rangle_{\text{V-plane}}}. \tag{2}$$

Optimising the directivity in the endfire direction, the resulting current distributions for each of the three quantities, D_{3D}, D_H and D_V, are derived in Appendix A by adopting the method developed in [36] to planar directivities of Eqn. (2). The optimum current ratio for the dimer I_2/I_1 can be presented in the general form

$$\left(\frac{I_2}{I_1}\right)_{\text{opt}} = \frac{ae^{iu} - b}{a - be^{iu}}. \tag{3}$$

This optimum current ratio will result in the maximum achievable directivity for the specified dimer, equal to

$$D_{\text{opt}} = 2\frac{a - b\cos(u)}{a^2 - b^2}. \tag{4}$$

where $u = kd$. Quantities a and b in Eqns. (3) and (4) take the following values, depending on which of the directivities, D_{3D}, D_H or D_V, is being optimised:

$$\begin{cases} a = \frac{2}{3}, & b = \frac{\sin u}{u} + \frac{\cos u}{u} - \frac{\sin u}{u^3} \quad \text{(3D)} \\ a = 1, & b = J_0(u) \quad \text{(H-plane)} \\ a = \frac{1}{2}, & b = J_0(u) - \frac{J_1(u)}{u} \quad \text{(V-plane)} \end{cases} \tag{5}$$

where $J_0(u)$ and $J_1(u)$ are the 0^{th} and 1^{st} order Bessel functions of the 1^{st} kind.

We focus on the $u \ll 1$ condition, so that $d \ll \lambda$ (small distance between the elements of the dimer).

Expanding Eqns. (3) and (4) in terms of u, we obtain, for the optimum current ratio,

$$\left(\frac{I_2}{I_1}\right)_{\text{opt}} = \begin{cases} -1 - j\frac{2}{5}u + \frac{2}{25}u^2 + j\frac{323}{10500}u^3 - \frac{239}{26250}u^4 + \ldots \\ \qquad \text{(3D)} \\ -1 - j\frac{1}{2}u + \frac{1}{8}u^2 + j\frac{1}{24}u^3 - \frac{5}{384}u^4 + \ldots \\ \qquad \text{(H-plane)} \\ -1 - j\frac{3}{4}u + \frac{9}{32}u^2 + j\frac{61}{768}u^3 - \frac{41}{2048}u^4 + \ldots \\ \qquad \text{(V-plane)} \end{cases} \tag{6}$$

and for the optimum directivity,

$$D_{\text{opt}} = \begin{cases} \frac{21}{4} - \frac{377}{1120}u^2 + \frac{541}{2822400}u^4 + \ldots & \text{(3D)} \\ 3 - \frac{1}{6}u^2 - \frac{1}{320}u^4 + \ldots & \text{(H-plane)} \\ \frac{14}{3} - \frac{35}{216}u^2 - \frac{1303}{155520}u^4 + \ldots & \text{(V-plane).} \end{cases} \tag{7}$$

It should be noted that the optimum currents are equal in magnitude and differ only in phase as follows from Eqn. (3).

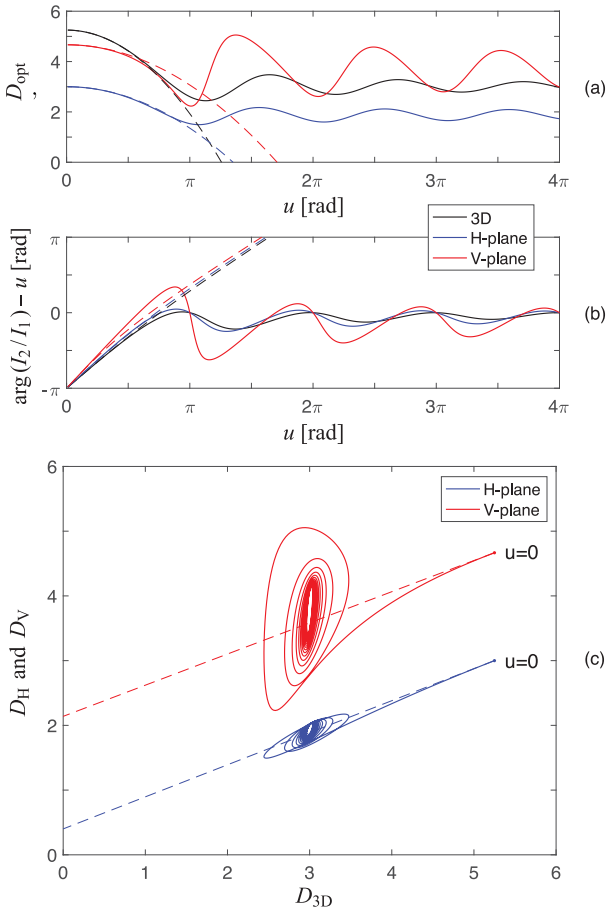

FIGURE 2. **(a) Optimum directivity and (b) the corresponding phase between the elements of the dimer with the value of u subtracted, versus $u = kd$. (c) Parametric curve: planar directivity versus 3D directivity. Black curves: 3D directivity. Blue curves: H-plane directivity. Red curves: V-plane directivity. Solid curves: exact solution. Dashed curves: Taylor series expansion up to the 2nd term.**

Figure 2(a) illustrates the variation of the optimum directivity with $u = kd$ for 3D (black curves), H-plane (blue curves) and V-plane (red curves). Solid curves are the exact solutions of Eqn. (4) and dashed curves are the Taylor series approximations of Eqn. (7). Figure 2(b) shows the corresponding phase difference between the currents I_2 and I_1, with the value of u subtracted, with solid curves showing the exact values of Eqns. (3) and the dashed curves the approximate values of Eqns. (6) with only the first two terms taken into account. Clearly the Taylor series approximation holds not only in the limit of $u \to 0$ but up to the value of $u \simeq \pi/2$ which corresponds to distance $d = \lambda/4$.

For very large values of u the optimum current distribution is close to that of a phased array - the phase difference between the currents I_1 and I_2 is close to u and the 3D directivity oscillates with u but stays close to the value of 3. Planar directivities follow a similar pattern.

As u tends to zero, however, the dimer configuration enters the superdirective regime with all three directivities, D_{3D}, D_H and D_V, growing monotonically as $u \to 0$ (see Fig. 2(a)). As can be seen from Fig. 2(b), in the superdirective regime, the angle between the currents of the dimer is no longer

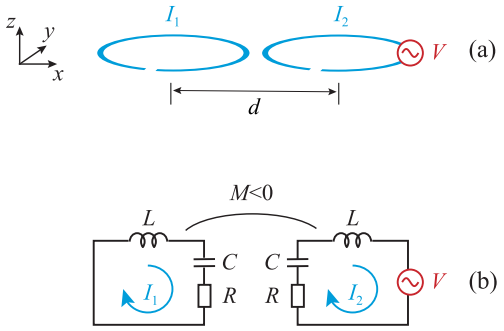

FIGURE 3. (a) Schematic representation of a dimer of coupled ring resonators with only one element being driven by external voltage. (b) The equivalent circuit.

equal to u; it approaches π as $u \to 0$, for 3D, H- and V-cases – the currents being nearly in anti-phase result in the destructive interference of the radiated fields leading to superdirectivity. Figure 2(c) shows the parametric plots D_{H} and D_{V} versus $D_{3\mathrm{D}}$. The superdirective regime is labelled as $u = 0$ in both cases.

Our goal is to see whether extracting information regarding planar directivity can be used as an indicator for the proper, 3D directivity and the result of Fig. 2 is encouraging. Especially the horizontal directivity D_{H} can be seen to be optimum at very similar values of the currents as the 3D directivity $D_{3\mathrm{D}}$ [see black and blue curves in Fig. 2(a)]. Hence we assume that by optimising the H-plane directivity we can simultaneously optimise the 3D directivity as well.

III. SUPERDIRECTIVITY CONDITIONS FOR COUPLED META-ATOMS

Knowing the superdirective current distribution, we shall now use the technique developed in [27] of realising this desired current condition by exciting only one of the meta-atoms and by choosing suitable values for the coupling constant and the quality factor of the elements. Assuming that the dipole approximation used in Section II is applicable for description of the radiative properties of the meta-atoms of the split-ring type shown schematically in Fig. 3(a), we can find the circuit properties of the elements by modelling them as identical resonant LCR circuits coupled via mutual inductance, M, with element 2 being driven by external voltage, V, as shown in Fig. 3(b). Note that for the planar arrangements of elements the mutual inductance is negative.

By writing the generalised Ohm's law for the dimer [27], the ratio of the currents as a function of the frequency can be written in the form

$$\frac{I_2}{I_1} = -\frac{2}{\kappa}\left(1 - \nu^2 - j\frac{\nu}{Q}\right) \tag{8}$$

where

$$\kappa = \frac{2M}{L}, \quad Q = \frac{\omega_0 L}{R}, \quad \omega_0 = \frac{1}{\sqrt{LC}} \text{ and } \nu = \frac{\omega_0}{\omega} \tag{9}$$

are the coupling constant between meta-atoms, the quality factor, the resonant frequency and the inverse of the normalised frequency of radiation, respectively. L is the self inductance, C is the capacitance and R is the resistance of each meta-atom. To achieve superdirectivity, the current ratio in Eqn. (8) should be equal to the optimum defined by Eqn. (6) up to the second term of the Taylor series valid for small u as previously discussed. We shall now see how the superdirective conditions for the 3D directivity, the H-plane directivity and the V-plane directivity compare:

$$-\frac{2}{\kappa}\left(1 - \nu^2 - j\frac{\nu}{Q}\right) = \begin{cases} -1 - j\frac{2}{5}u & \text{(3D)} \\ -1 - j\frac{1}{2}u & \text{(H-plane)} \\ -1 - j\frac{3}{4}u & \text{(V-plane).} \end{cases} \tag{10}$$

Equating the real parts of Eqns. (6) and (8) we find the superdirective condition 1 which prescribes at what frequency the dimer can be superdirective:

$$\frac{\kappa}{2} = 1 - \nu^2 \quad (\mathrm{SD}_1 \text{ condition}). \tag{11}$$

SD_1 condition can be seen to be identical for all three quantities of interest, for the 3D directivity, the H-plane directivity and the V-plane directivity. Rewriting Eqn. (11) as

$$\frac{\omega}{\omega_0} = \frac{1}{\sqrt{1 - \kappa/2}} \quad (\mathrm{SD}_1 \text{ condition}) \tag{12}$$

we can conclude that in order to achieve the optimum directivity (3D, H-plane and V-plane) the operating frequency has to be tuned to the resonance frequency of the antisymmetric mode for two coupled meta-atoms [37] at which both currents are nearly in anti-phase, just as required for the destructive interference mechanism of superdirectivity.

It is an important result that the SD_1 condition is the same for all three types of directivity, verifying that by choosing the operating frequency optimising planar directivity we are simultaneously optimising the 3D directivity as well. This condition is necessary but not sufficient for realising superdirectivity with a dimer of two coupled meta-atoms.

The other necessary condition is obtained by equating the imaginary parts of Eqns. (8) and (6) and substituting Eqn. (11) as:

$$\frac{|\kappa| Q}{\sqrt{1 - \kappa/2}} = \begin{cases} \frac{5}{kd} & \text{(3D)} \\ \frac{4}{kd} & \text{(H-plane)} \\ \frac{8}{3kd} & \text{(V-plane)} \end{cases} \quad (\mathrm{SD}_2 \text{ condition}) \tag{13}$$

where we took into account that $\kappa < 0$ for the split-ring resonators placed side by side in the xy plane. This relationship prescribes the required values of κ and Q for a dimer to exhibit superdirective behaviour. As can be seen the SD_2 condition is different for the three quantities of interest (3D, H-plane and V-plane directivities).

We have also repeated the same calculations for isotropic radiators (see Appendix B). We have found that the H-plane and V-plane directivities (which are for isotropic radiators equal to each other) are optimised at the same value of $|\kappa| Q = 4/kd$ as the H-plane directivity of the dipoles. As shown in [27] for an isotropic dimer structure, the RHS of Eqn. (13) (3D case) modifies to $6/kd$ which differs from the value of $5/kd$ for dipoles. This suggests that if in an experiment we would

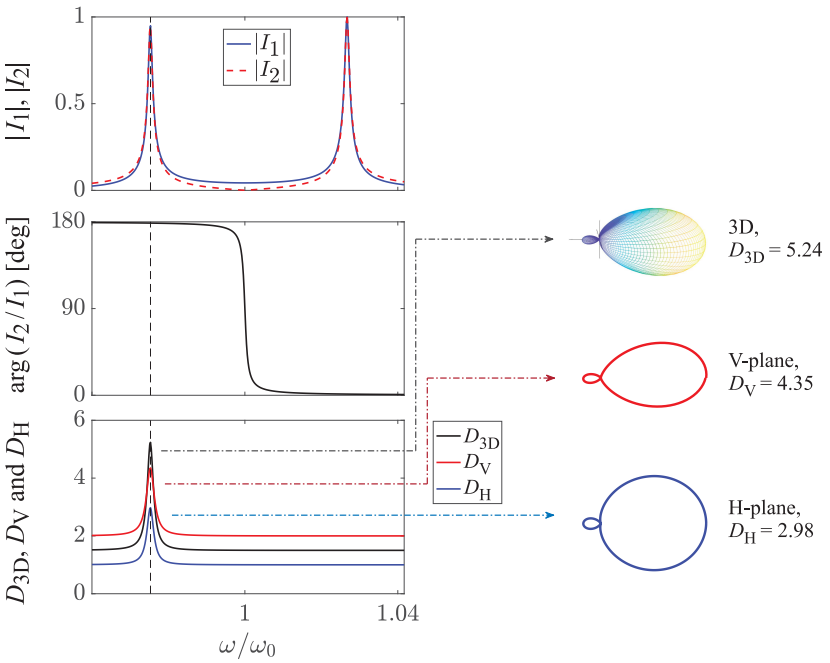

FIGURE 4. Frequency variation for the amplitude and phase (top two panes on the left) of dimer's currents and the resulting 3D directivity, H-plane directivity and V-plane directivity (bottom left). On the RHS: The 3D radiation patterns and H-plane and V-plane radiation patterns at the optimum frequency. $Q = 880$, $f_0 = 110$ MHz, $d = 24$ mm, $\kappa = -0.1$.

optimise planar directivity according to the SD_2 condition the expected error in determining the optimum conditions for the 3D directivity will depend on the actual shape of the elements and on their individual radiation patterns. We will analyse the discrepancies in more detail in Section IV. Examples in Fig. 4 illustrate that simultaneously satisfying SD_1 and SD_2 condition does result in superdirectivity. We choose the following set of parameters: $f_0 = \omega_0/2\pi = 110$ MHz, $Q = 880$, $d = 24$ mm and $\kappa = -0.1$. This set satisfies the SD_2 condition for the 3D directivity. We plot in Fig. 4 the currents (absolute values and the phases) and the resulting 3D, H-plane and V-plane directivities as a function of frequency. Clearly, D_{3D}, D_H and D_V reach their maximum at a frequency very close to the lower resonance as predicted by the SD_1 condition. We also show the resulting radiation patterns in 3D, in the H-plane and in the V-plane at the optimum frequency. The 3D directivity reaches the value of 5.24 which matches the theoretical maximum for the given set of parameters. The corresponding H-plane directivity is 2.98, also very close to its theoretical maximum, and the V-plane directivity is not far off either at 4.35.

So far our findings confirm our conclusions that it would be feasible in a lab environment to resort to a simplified procedure of measuring planar directivities and optimising the setup without the need of capturing the 3D radiation pattern.

IV. SIMULATIONS

We performed numerical simulations for realistic meta-atoms using the time domain solver of CST Microwave Studio®. The goal was to verify our hypothesis that by optimising planar directivity we are able to identify the optimum for the actual 3D directivity. Only one of the two meta-atoms was excited by placing a current source into its gap. The mesh was adjusted to ensure that both the accuracy and the computational time are reasonable. We simulated circular and square copper split-ring resonators shown schematically in Fig. 5. Flat circular and square shaped resonators have been extensively studied from the early advent of metamaterials research [38], [39], with applications involving superdirectivity [36]. These two types of elements are of equal outer dimension, 23mm, with the same wall thickness $w = 1$ mm, same height $h = 5$ mm and same gap $g = 2$ mm, into which a suitable capacitor is inserted enabling resonant frequency tuning. As shown in [27], these split-pipe resonators do not behave exactly as magnetic dipoles and the optimum 3D directivity is achieved at $|\kappa|Q/\sqrt{1-\kappa/2} = 4/kd$ both for circular and for square resonators.

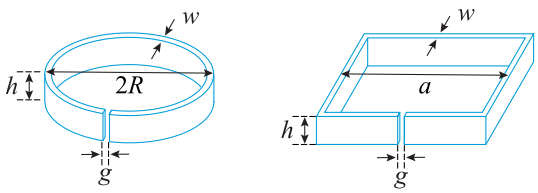

FIGURE 5. Circular and square split-pipe resonators used in simulations.

As far as the H-plane directivity is concerned, here we expect that our analytical predictions will be valid due to the rotational symmetry of the radiated fields. This assumption is supported by the fact that analytically the H-plane directivity for isotropic radiators also gave the same SD_2 condition, $|\kappa|Q/\sqrt{1-\kappa/2} = 4/kd$.

We explore now two scenarios, in the first one we keep the distance between the resonators constant and vary the

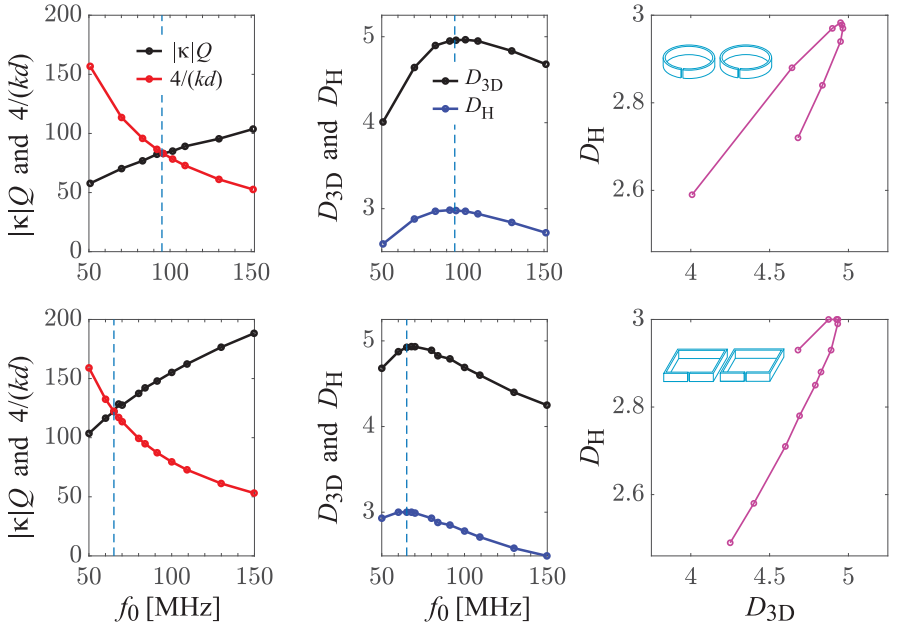

FIGURE 6. Optimising dimer's directivity for a specified geometry as a function of resonant frequency. Top row: circular split pipes with $2R = 23$ mm, $d = 24$ mm, $\kappa = -0.1$. Bottom row: square elements with $a = 23$ mm, $d = 24$ mm, $\kappa = -0.19$. Left column: LHS ($|\kappa|Q$) and RHS ($4/kd$) of SD_2. Crossing point of solid and dashed curves indicate the expected optimum resonant frequency. Central column: variation of D_{3D} and D_H with resonant frequency confirms the validity of SD_2 yielding maximum directivity at the expected frequency. Right column: parametric plot D_H vs. D_{3D} confirming that both reach maximum at almost the same frequency.

resonant frequency and in the second one we keep the resonant frequency constant and vary the distance between the resonators.

In the first set of simulations, the centre-to-centre distance, d, was kept constant at 24 mm. The coupling constant is $\kappa = -0.1$ for the dimers of circular elements and -0.19 for the dimers of square elements as calculated following the procedure detailed in [40]. By varying the added capacitance, f_0 was varied from 50 to 150 MHz. In Fig. 6, the upper row shows the results for circular elements, and the lower row for the square elements. The first column on the left in Fig. 6 shows the variation of the $|\kappa|Q$ and $4/u$, which are the LHS and RHS of the SD_2 condition for the H-plane directivity. The frequency at which both curves intersect is the optimum resonant frequency that should yield superdirectivity both for the H-plane and for 3D; we mark this point by the vertical dashed line. For circular meta-atoms the optimum frequency value is 95 MHz and for square meta-atoms it is 65 MHz.

The variation of the optimum 3D directivity and optimum H-plane directivity with the resonant frequency is shown in the central column of Fig. 6. The maximum position for both 3D and H-plane directivities agree well with the predictions of the model. For circular elements, the optimum frequency is 92 MHz for the H-plane directivity and 101 MHz for 3D directivity. This amounts to a 9% error in the value of the optimum frequency. For square elements, the optimum frequency is 60 MHz for the H-plane directivity and 68 MHz for 3D directivity. This amounts to a 12% error in the value of the optimum frequency. How large would be the actual error for the directivity itself if we were to use the optimum frequency relying on a planar measurement? We define ΔD as the error in evaluating directivity at the H-plane optimum frequency rather than at the correct optimum frequency:

$$\Delta D = \left| \frac{D(f|_{D_{\mathrm{H,max}}}) - D_{\mathrm{max}}}{D_{\mathrm{max}}} \right|. \tag{14}$$

From the data shown in the central column of Fig. 6 we calculate ΔD to be equal to 0.4 % for circular and 0.6% for square elements. The errors in the values of the directivity are significantly lower than the errors in the frequencies. This robustness against frequency variation is due to a flat maximum in the frequency dependence of both directivities, D_H and D_{3D}. The parametric plots in the right column of Fig. 6 use the values of the directivities, D_H and D_{3D}, at the optimum frequency which coincided with the SD_1 condition illustrating that the condition for the 3D directivity and for the H-plane directivity are practically the same. Our conclusion so far is that in this numerical study, optimising solely the H-plane directivity and adjusting the resonant frequency until the optimum is found, we succeeded in optimising the 3D directivity. In the lab this procedure would have allowed us to avoid a lengthy 3D measurement of the radiation pattern requiring just measurements in the azimuthal xy plane. The discrepancy in the achieved value of the 3D directivity of less than 0.6% validates our approach.

In the next series of simulations (Fig. 7) we kept the resonant frequency constant and varied the distance between the elements of the dimer. Fig. 7 is organised in the same way as Fig. 6, only the parameter varying is the centre-to-centre distance, d, instead of the resonant frequency, f_0. The intersection of the $|\kappa|Q$ and $4/u$ curves, which are the LHS and RHS of the SD_2 condition respectively (plotted in

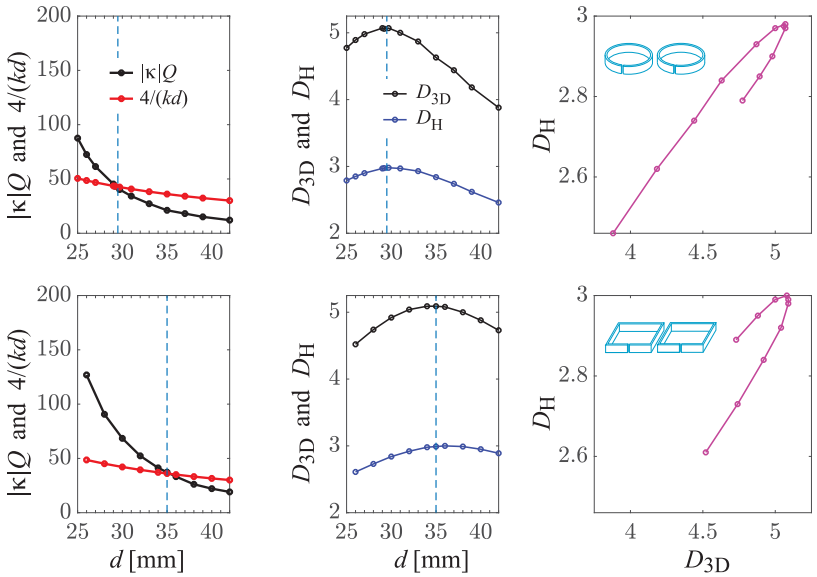

FIGURE 7. Optimising dimer's directivity for a specified resonant frequency as a function of distance between meta-atoms. Top row: circular split pipes with $2R = 23$ mm, $f_0 = 150$ MHz, $Q = 1000$. Bottom row: square elements with $a = 23$ mm, $f_0 = 150$ MHz, $Q = 750$. Left column: LHS ($|\kappa|Q$) and RHS ($4/kd$) of SD_2. Crossing point of solid and dashed curves indicate the expected optimum centre-to-centre distance between split pipes. Central column: variation of D_{3D} and D_H with distance confirms the validity of SD_2 yielding maximum directivity at the expected distance. Right column: parametric plot D_H vs. D_{3D} confirming that both reach maximum at almost the same distance.

the first column of Fig. 7) suggests the optimum distance of 29 mm for circular elements and of 35 mm for square elements. The numerically obtained values of the H-plane directivity and of the 3D directivity confirm our expectations with good accuracy. For circular elements, the optimum distance is 30 mm for the H-plane directivity and 29 mm for 3D directivity. For square elements, the optimum distance is 36 mm for the H-plane directivity and 35 MHz for 3D directivity. In both cases, this amounts to a 3% error in the value of the optimum distance. Using Eqn. (14), the error in directivity is estimated to be again significantly lower, less than 0.2% for both configurations. We conclude that also in this case the measurements and optimisation of the H-plane directivity would have enabled us to identify the best configuration with respect to the distance between the elements of the dimer.

V. CONCLUSION

A rapid way of optimising directivity is developed that results in superdirective performance of metamaterial-inspired end-fire dimers with strong inter-element coupling with only one element driven. Our method is in optimising not the 3D directivity but its planar equivalent. An analytical model derived for coupled magnetic dipoles predicts that it is permissible to rely on simple 2D measurements of planar directivity to optimise the set-up. The aim is to satisfy the superdirective conditions by imposing rules, for any given distance between the elements, upon the quality factor and the coupling constant. Our analytical model is verified numerically for dimers of split-pipe resonators of extended height that mimic 3D-printed resonators of circular or square shape. For both varieties (circular or square) we found numerical simulations to be in full agreement with the predictions of the analytical model.

We expect that our approach would be suitable for meta-atoms of different shape. In particular, with the advent of additive manufacturing, 3D-printed meta-atoms gain in importance and our method would enable rapid evaluation of the superdirective performance of 3D-printed arrays and would aid rapid prototyping of 3D-printed arrays with radiative properties on demand.

Superdirectivity realised by metamaterial elements has a number of advantages over other realisations, e.g., that it is not necessary to excite separately all the elements. But this realisation shares the common property of all superdirective antennas, namely narrow bandwidth, high tolerance sensitivity and low efficiency. Superdirective antennas are used in cases when high directivity (narrow beams in order to avoid electromagnetic pollution) is preferred over efficiency. By generalising the method developed in the present paper for use at higher frequencies will enable us to achieve reasonable radiation efficiency [25]. The method developed in the present paper assumed that the elements can be treated as simple magnetic dipoles with real coupling constant. For higher frequencies, retardation effects would need to be incorporated into the model. A possible further step could be to generalise the model to account for retardation and the possibility of both magnetic and electric coupling and by modelling the split ring as a combination of a magnetic and an electric dipole. This generalisation would enable to describe a wider range of meta-atoms including omega-particles.

Finally, the method developed in this paper can also be applied to optimising broadside directivity [36], [41], and might even be used in predicting and optimising array directivities outside the field of superdirectivity. Although achievable broadside array directivities are more modest in magnitude than end-fire array directivities, broadside arrays are widely used in practice hence a rapid optimisation tool developed

in the present paper may aid design and implementation of this family of metamaterial-based antenna arrays.

APPENDIX A
OPTIMUM CURRENT AND MAXIMUM DIRECTIVITY

We derive in this Appendix expressions used in Section II by adopting the approach developed in [5], [27], [36] that enables a compact neat way of operating with matrix quantities.

Referring to Fig. 1, to characterise the direction $\mathbf{i_r}$ in which we wish to determine the power density radiated by the dimer, we shall use two sets of spherical coordinates - (θ, φ) which is related to the dipole axis (z direction), and (θ', φ'), related to the axis of the array (x axis). Elevation angle θ is the angle between the z axis and $\mathbf{i_r}$, and azimuthal angle φ the angle between the x axis and the projection of $\mathbf{i_r}$ onto the xy plane. Similarly, elevation angle θ' is the angle between the x axis and $\mathbf{i_r}$, and azimuthal angle φ' is the angle between the y axis and the projection of the radius vector onto the yz plane. Hence

$$\mathbf{i_r} = \begin{pmatrix} \sin\theta\cos\varphi \\ \sin\theta\sin\varphi \\ \cos\theta \end{pmatrix} = \begin{pmatrix} \cos\theta' \\ \sin\theta'\cos\varphi' \\ \sin\theta'\sin\varphi' \end{pmatrix}. \tag{15}$$

We define the inner product of two vectors as

$$\mathbf{ab} = \sum_{n=1}^{2} a_n b_n^* \tag{16}$$

and the outer product producing a matrix $\mathbf{c}$ as

$$c_{mn} = a_m b_n^*. \tag{17}$$

The inner product of a matrix and a vector yields a vector

$$a_m = c_{mn} b_n^*. \tag{18}$$

Using these notations, we can write the electric field strength in the far field produced by a dimer of identical meta-atoms placed at a distance d along the x axis as the inner product of two vectors

$$\mathbf{E} = C\mathbf{FI} \tag{19}$$

where C is a constant,

$$\mathbf{I} = [I_1 \quad I_2] \tag{20}$$

is the current distribution in the two elements and

$$\mathbf{F} = \sin\theta\left[1, \quad e^{ju\sin\theta\cos\varphi}\right] \tag{21}$$

indicates the geometry of the dimer structure. The power density is then of the form

$$P_\mathrm{d} = \frac{|E|^2}{2Z_0} = \frac{C^2}{2Z_0}\mathbf{IBI} \tag{22}$$

where matrix $\mathbf{B}$ is the outer product of $\mathbf{F}$ with itself

$$\mathbf{B} = \mathbf{F} \circ \mathbf{F}. \tag{23}$$

The average power density is given by

$$\langle P \rangle = \frac{C^2}{2Z_0}\mathbf{IAI} \tag{24}$$

where averaging is either over the solid angle 4π for 3D directivity, or over angle α within the H- or V-plane:

$$\mathbf{A} = \begin{cases} \frac{1}{4\pi}\int_0^{2\pi}\int_0^{\pi} \mathbf{B}\sin\theta d\theta d\varphi & \text{(3D directivity)} \\ \frac{1}{2\pi}\int_0^{2\pi} \mathbf{B}d\alpha|_{\text{H-plane}} & \text{(H-plane directivity)} \\ \frac{1}{2\pi}\int_0^{2\pi} \mathbf{B}d\alpha|_{\text{V-plane}} & \text{(V-plane directivity).} \end{cases} \tag{25}$$

The results of the integration which is easier to perform when transforming to the coordinates (θ', φ') from Eqn. (15) are summarised for all there cases (3D, H-plane, and V-plane) in Eqn. (5) where $a = A_{11} = A_{22}$ and $b = A_{12} = A_{21}$.

The directivity is then

$$D = \frac{\mathbf{IBI}}{\mathbf{IAI}} \tag{26}$$

where $\mathbf{B}$ is evaluated in the $\theta = \pi/2$, $\varphi = 0$ direction, the direction of maximum radiation. The optimum current is given as [5]

$$\mathbf{I}_\mathrm{opt} = \mathbf{A}^{-1}\mathbf{F} \tag{27}$$

and the maximum available directivity is

$$D_\mathrm{opt} = \mathbf{FA}^{-1}\mathbf{F}. \tag{28}$$

APPENDIX B
OPTIMISATION FOR ISOTROPIC RADIATORS

To provide more context with regard to the role individual radiation patterns might play, in this Appendix we apply our method to the case of coupled isotropic radiators placed at a distance d, aiming at optimising radiation in the end-fire direction. For isotropic radiators Eqn. (21) may be rewritten as

$$\mathbf{F} = \left[1, \quad e^{ju\sin\theta\cos\varphi}\right]. \tag{29}$$

For symmetry reasons, in the case of isotropic radiators there is no difference between the horizontal and the vertical planar directivity,

$$D_\mathrm{H} = D_\mathrm{V} = D_\mathrm{planar}. \tag{30}$$

The elements of matrix A, a and b, needed for Eqns. (3) and (4), take the following values for the 3D and planar directivity:

$$\begin{cases} a = 1, & b = \frac{\sin u}{u} \quad \text{(3D isotropic)} \\ a = 1, & b = J_0(u) \quad \text{(planar isotropic).} \end{cases} \tag{31}$$

Substituting Eqn. (31) into Eqns. (3) and (4) and expanding the resulting expressions in terms of $u \ll 1$ we obtain for the optimum current ratio in the case of isotropic radiators,

$$\left(\frac{I_2}{I_1}\right)_\mathrm{opt} = \begin{cases} -1 - j\frac{1}{3}u + \frac{1}{18}u^2 + j\frac{7}{270}u^3 - \frac{23}{3240}u^4 + \ldots \\ \qquad \text{(3D isotropic)} \\ -1 - j\frac{1}{2}u + \frac{1}{8}u^2 + j\frac{1}{24}u^3 - \frac{5}{384}u^4 + \ldots \\ \qquad \text{(planar isotropic)} \end{cases} \tag{32}$$

and for the maximum achievable directivities,

$$D_\mathrm{opt} = \begin{cases} 4 - \frac{4}{15}u^2 + \frac{4}{1575}u^4 + \ldots & \text{(3D isotropic)} \\ 3 - \frac{1}{6}u^2 - \frac{1}{320}u^4 + \ldots & \text{(planar isotropic)} \end{cases}. \tag{33}$$

It should be noted that, similarly to the case of coupled dipoles, the optimum currents turn out to be equal in magnitude and differ only in phase as follows from Eqn. (3). We also note that the expressions for the optimum current and optimum directivity in the case of planar directivity for isotropic radiators coincide with the case of horizontal directivity for the dipoles, see Eqns. (5)-(7) and Eqns. (31)-(33). This is not surprising as dipoles have isotropic radiation pattern in the horizontal plane.

DATA AVAILABILITY

The research materials supporting this publication can be accessed by contacting the corresponding author: Jiaruo Yan (e-mail: jiaruo.yan@eng.ox.ac.uk).

ACKNOWLEDGMENT

The authors would like to thank Dr. A. Vallecchi and colleagues from the OxiMeta Oxford University Network on Metamaterials for the fruitful discussions.

REFERENCES

[1] C. W. Oseen, "Die einsteinsche nadelstichstrahlung und die maxwellschen gleichungen," *Ann. d. Phys.*, vol. 69, no. 19, pp. 202–204, 1922.
[2] S. A. Schelkunoff, "A mathematical theory of linear arrays," *Bell Syst. Techn. J.*, vol. 22, no. 1, pp. 80–107, 1943.
[3] A. I. Uzkov, "An approach to the problem of optimum directive antenna design," *Compt. Rend. Dokl. Acad. Sci. USSR*, vol. 53, no. 1, pp. 35–38, 1946.
[4] A. Bloch, R. G. Medhurst, and S. D. Pool, "A new approach to the design of super-directive aerial arrays," *Proc. IEE III, Radio Commun. Eng.*, vol. 100, no. 67, pp. 303–314, Sep. 1953.
[5] M. Uzsoky and L. Solymar, "Theory of super-directive linear arrays," *Acta Physica Acad. Hung. Sci.*, vol. 6, pp. 185–205, Dec. 1956.
[6] G. Toraldo di Francia, "Super-gain antennas and optical resolving power," *Il Nuovo Cimento (1943-1954)*, vol. 9, pp. 426–438, Mar. 1952.
[7] L. J. Chu, "Physical limitations of omni-directional antennas," *J. Appl. Phys.*, vol. 19, no. 12, pp. 1163–1175, 1948.
[8] R. F. Harrington, "Effect of antenna size on gain, bandwidth, and efficiency," *J. Res. Nat. Bureau Stand*, vol. 64, no. 1, pp. 1–12, 1960.
[9] D. M. Pozar, "New results for minimum Q, maximum gain, and polarization properties of electrically small arbitrary antennas," in *Proc. 3rd Eur. Conf. Antennas Propag. (EuCAP)*, Berlin, Germany, Mar. 2009, pp. 1993–1996.
[10] L. Solymar, "Maximum gain of a line source antenna if the distribution fuction is a finite fourier series," *IRE Trans. Antennas Propag.*, vol. 6, no. 3, pp. 215–219, Jul. 1958.
[11] C. T. Tai, "The optimum directivity of uniformly spaced broadside arrays of dipoles," *IEEE Trans. Antennas Propag.*, vol. 12, no. 4, pp. 447–454, Jul. 1964.
[12] Y. T. Lo, S. W. Lee, and Q. H. Lee, "Optimization of directivity and signal-to-noise ratio of an arbitrary antenna array," *Proc. IEEE*, vol. 54, no. 8, pp. 1033–1045, Aug. 1966.
[13] D. K. Cheng, "Optimization techniques for antenna arrays," *Proc. IEEE*, vol. 59, no. 12, pp. 1664–1674, Dec. 1971.
[14] S. M. Sanzgiri and J. K. Butler, "Constrained optimization of the performance indices of arbitrary array antennas," *IEEE Trans. Antennas Propag.*, vol. 19, no. 4, pp. 493–498, Jul. 1971.
[15] D. R. Rhodes, "On an optimum line source for maximum directivity," *IEEE Trans. Antennas Propag.*, vol. 19, no. 4, pp. 485–492, Jul. 1971.
[16] J. M. Bacon and R. G. Medhurst, "Superdirective aerial array containing only one fed element," *Proc. Inst. Elect. Eng.*, vol. 116, no. 3, pp. 365–372, Mar. 1969.
[17] E. H. Newman and M. R. Schrote, "A wide-band electrically small superdirective array," *IEEE Trans. Antennas Propag.*, vol. 30, no. 6, pp. 1172–1176, Nov. 1982.
[18] E. E. Altshuler, T. H. O'Donnell, A. D. Yaghjian, and S. R. Best, "A monopole superdirective array," *IEEE Trans. Antennas Propag.*, vol. 53, no. 8, pp. 2653–2661, Aug. 2005.
[19] A. D. Yaghjian, T. H. O'Donnell, E. E. Altshuler, and S. R. Best, "Electrically small supergain end-fire arrays," *Radio Sci.*, vol. 43, pp. 1–13, Jun. 2008.
[20] S. Lim and H. Ling, "Design of a closely spaced, folded Yagi antenna," *IEEE Antennas Wireless Propag. Lett.*, vol. 5, pp. 302–305, 2006.
[21] K. Buell, H. Mosallaei, and K. Sarabandi, "Metamaterial insulator enabled superdirective array," *IEEE Trans. Antennas Propag.*, vol. 55, no. 4, pp. 1074–1085, Apr. 2007.
[22] B. A. Panchenko, "Metamaterials and superdirectivity of antennas," *J. Commun. Technol. Electron.*, vol. 54, pp. 286–291, Mar. 2009.
[23] T. Kokkinos and A. P. Feresidis, "Electrically small superdirective endfire arrays of metamaterial-inspired low-profile monopoles," *IEEE Antennas Wireless Propag. Lett.*, vol. 11, pp. 568–571, 2012.
[24] E. Shamonina and L. Solymar, "Superdirectivity by virtue of coupling between meta-atoms," in *Proc. IEEE 7th Int. Congr. Adv. Electromagn. Mater. Microw. Opt. (Metamaterials 2013)*, Talence, France, Sep. 2013, pp. 97–99.
[25] A. Radkovskaya, A. Vallecchi, L. Li, G. Faulkner, C. Stevens, and E. Shamonina, "Experimental demonstration of superdirectivity for coupled dimers of meta-atoms," in *Proc. IEEE 10th Int. Congr. Adv. Electromagn. Mater. Microw. Opt. (Metamaterials 2016)*, Chania, Greece, Sep. 2016, pp. 328–330.
[26] E. Shamonina and L. Solymar, "Superdirective 'meta-molecules'," in *Proc. IEEE 8th Int. Congr. Adv. Electromagn. Mater. Microw. Opt. (Metamaterials 2014)*, Copenhagen, Denmark, Sep. 2014, pp. 268–279.
[27] A. Radkovskaya *et al.*, "Superdirectivity from arrays of strongly coupled meta-atoms," *J. Appl. Phys.*, vol. 124, pp. 1–11, Sep. 2018.
[28] A. Ludwig, C. D. Sarris, and G. V. Eleftheriades, "Metascreen-based superdirective antenna in the optical frequency regime," *Phys. Rev. Lett.*, vol. 109, pp. 1–4, Nov. 2012.
[29] R. J. Mailloux, *Phased Array Antenna Handbook*, 3rd ed. Norwood, MA, USA: Artech House, 2017.
[30] D. Margetis, G. Fikioris, J. M. Myers, and T. T. Wu, "Highly directive current distributions: General theory," *Phys. Rev. E*, vol. 58, no. 2, p. 2531, 1998.
[31] R. C. Hansen, *Electrically Small Superdirective and Superconducting Antennas*. New York, NY, USA: Wiley, 2006.
[32] E. Shamonina, V. A. Kalinin, K. H. Ringhofer, and L. Solymar, "Magnetoinductive waves in one, two, and three dimensions," *J. Appl. Phys.*, vol. 92, pp. 6252–6261, Oct. 2002.
[33] S. F. Razavi, S. Xu, T. Brockett, and Y. Rahmat-Samii, "The spillover effect on the directivity calculation of reflector antennas in planar near-field measurements [measurements corner]," *IEEE Antennas Propag. Mag.*, vol. 51, no. 6, pp. 124–134, Dec. 2009.
[34] F. Ferrara, C. Gennarelli, R. Guerriero, G. Riccio, and C. Savarese, "Computation of antenna directivity from cylindrical near-field measurements," *Microw. Opt. Techn. Lett.*, vol. 48, no. 4, pp. 686–691, 2006.
[35] O. Breinbjerg, "Spherical near-field antenna measurements—The most accurate antenna measurement technique," in *Proc. IEEE Int. Symp. Antennas Propag. (APSURSI)*, Fajardo, Puerto Rico, 2016, pp. 1019–1020.
[36] E. Shamonina and L. Solymar, "Maximum directivity of arbitrary dipole arrays," *IET Microw. Antennas Propag.*, vol. 9, no. 2, pp. 101–107, Jan. 2015.
[37] L. Solymar and E. Shamonina, *Waves in Metamaterials*. Oxford, U.K.: Oxford Univ. Press, 2009.
[38] K. Aydin, I. Bulu, K. Guven, M. Kafesaki, C. M. Soukoulis, and E. Ozbay, "Investigation of magnetic resonances for different split-ring resonator parameters and designs," *New J. Phys.*, vol. 7, pp. 1–15, Aug. 2005.
[39] M. Kafesaki, T. Koschny, R. S. Penciu, T. F. Gundogdu, E. N. Economou, and C. M. Soukoulis, "Left-handed metamaterials: Detailed numerical studies of the transmission properties," *J. Opt. A, Pure Appl. Opt.*, vol. 7, pp. S12–S22, Jan. 2005.
[40] E. Tatartschuk, N. Gneiding, F. Hesmer, A. Radkovskaya, and E. Shamonina, "Mapping inter-element coupling in metamaterials: Scaling down to infrared," *J. Appl. Phys.*, vol. 111, pp. 1–9, May 2012.
[41] E. Shamonina, K. H. Ringhofer, and L. Solymar, "Configurations optimizing the directivity of planar arrays," *AEU Int. J. Electron. Commun.*, vol. 56, no. 2, pp. 115–119, 2002.